Confined quantum systems: spectral properties of two-electron quantum dots

2003 J. Phys.: Condens. Matter 15 5487

(http://iopscience.iop.org/0953-8984/15/32/310)

INSTITUTE OF PHYSICS PUBLISHING JOURNAL OF PHYSICS: CONDENSED MATTER

J. Phys.: Condens. Matter **15** (2003) 5487–5509 PII: S0953-8984(03)62508-7

Confined quantum systems: spectral properties of two-electron quantum dots

T Sako and G H F Diercksen[1]

Max-Planck-Institut für Astrophysik, Karl-Schwarzschild-Strasse 1, D-85741 Garching, Germany

Received 22 April 2003
Published 1 August 2003
Online at stacks.iop.org/JPhysCM/15/5487

Abstract

The spectrum, electron-density distribution and ground-state correlation energy of two electrons confined by an anisotropic harmonic oscillator potential have been studied for different confinement strengths ω by using the quantum chemical configuration interaction (CI) method employing a large Cartesian anisotropic Gaussian basis set and a full CI wavefunction. Energy level diagrams and electron-density distributions are displayed for selected electronic states and confinement parameters. The total energy and spacing between energy levels increase in all cases with increasing ω. The energy level structure cannot be matched by scaling with respect to ω. The correlation energy of the ground state is comparable in magnitude to that of the helium atom. It increases for increasing ω. The percentage of the correlation energy with respect to the total energy of the ground state is considerably larger than that of the helium atom.

1. Introduction

Recent advances in semiconductor technology have allowed the construction of new quantum systems, sometimes referred to as artificial atoms [1] or quantum dots [2, 3]. An artificial atom is essentially a number of electrons confined in a potential well. Another area where spatial confinement leads to the appearance of new properties of quantum systems is the embedding of atoms and molecules in nano-cavities, as for example in zeolite cages [4], fullerenes [5, 6] and in nano-bubbles formed around foreign objects in the environment of liquid helium [7], etc.

Studies of quantum objects confined by different forms of external potentials have attracted the attention of both physicists and quantum chemists since the early days of quantum mechanics. The Schrödinger equation for an electron in a uniform magnetic field confined by a harmonic oscillator type potential was solved already in 1928 by Fock [8] and investigated two years later again by Darwin [9]. Since then numerous studies on a variety of confining

[1] Author to whom any correspondence should be addressed.

0953-8984/03/325487+23$30.00

potentials have been published. Special attention has been paid to those potentials which allow for analytical solutions of the eigenvalue problem of the corresponding Hamiltonian. But only recently analytical solutions have been obtained for two interacting electrons in an external harmonic oscillator potential [10–12].

The development of new technologies and experimental techniques has triggered intensive theoretical studies on modelling spatially confined quantum systems. A review by Jaskólski gives a broad account of these studies prior to 1996 [13]. A rather complete list of later studies on confined atoms may be found in a recent paper by Connerade *et al* [14]. Most of the previous studies are concerned with one-electron systems [15–22] or with many-electron atoms described at the Hartree–Fock (HF) level [13, 14, 23]. Studies of the effect of electron correlation in confined many-electron systems are still limited [24–27]. Special attention has been paid recently to the study of quantum dots [10, 12, 23–39]. The form of confinement studied has been rather restricted. An infinite rectangular potential well [15, 17, 38, 40–42] or other potential wells for which the potential is infinite outside of a certain range of coordinates have been used in the majority of cases. The harmonic oscillator potential has been used in most of the investigations of quantum dots. Most studies are limited to ground-state properties. Only very recently results of several studies on the influence of electron correlation effects and of the form of the confinement on the spectral properties of the confined system have been published [43–47].

In this, and in subsequent studies, quantum-chemical models of atoms and molecules are applied to investigate the effects of spatial confinement on the properties and reactions of quantum systems. The confined object is described by the HF and configuration interaction (CI) methods. The spatial confinement is defined by an external one-particle potential introduced to the N-electron Hamiltonian. The present contribution reports the spectral properties of the low lying singlet states of a two-electron quantum dot confined by an anisotropic harmonic oscillator potential. The results for the triplet states will be reported elsewhere [48]. The spectrum is studied for different geometry and confinement strength ω. Energy level diagrams and electron-density distributions are displayed for selected electronic states and confinement parameters of the quantum dot. Atomic units are used in this paper.

2. Computational methodology

2.1. A short review of electrons in a harmonic oscillator potential

The Schrödinger equation for N electrons confined by a potential $\mathcal{W}$ is given by (in atomic units)

$$[\mathcal{H}(\boldsymbol{r}) + \mathcal{W}(\boldsymbol{r})]\Psi(1, 2, \ldots, N) = E\Psi(1, 2, \ldots, N), \tag{1}$$

where the set $(1, 2, \ldots, N)$ denotes the orbital and the spin coordinates of the electrons. The N-electron operators $\mathcal{H}$ represents the kinetic energy and the electron interaction described by

$$\mathcal{H}(\boldsymbol{r}) = \sum_{i=1}^{N}\left[-\frac{1}{2}\nabla_i^2\right] + \sum_{i>j}^{N}\left[\frac{1}{|\boldsymbol{r}_i - \boldsymbol{r}_j|}\right], \tag{2}$$

where $\boldsymbol{r} \equiv \{\boldsymbol{r}_1, \boldsymbol{r}_2, \ldots, \boldsymbol{r}_N\}$ denotes the spatial coordinates of the electrons. The N-electron interaction potential $\mathcal{W}$ is defined as the sum of one-electron contributions:

$$\mathcal{W}(\boldsymbol{r}) = \sum_{i=1}^{N} w(\boldsymbol{r}_i). \tag{3}$$

The one-particle confining potential $w(\boldsymbol{r}_i)$ is written as a linear combination of powers of electron coordinates:

$$w(\boldsymbol{r}_i) = \tfrac{1}{2}[\omega_x^{n_x+1} x_i^{2n_x} + \omega_y^{n_y+1} y_i^{2n_y} + \omega_z^{n_z+1} z_i^{2n_z}], \tag{4}$$

where $\boldsymbol{r}_i = \{x_i, y_i, z_i\}$. The potential of equation (4) allows for the description of a wide variety of physical situations, including quantum systems confined in spheres, ellipsoids and (nano)tubes. All calculations in the present study have been performed for an anisotropic harmonic oscillator potential centred at the origin of the coordinate system ($n_x = n_y = n_z = 1$):

$$V_{\boldsymbol{\omega}}(\boldsymbol{r}) = \tfrac{1}{2}(\omega_x^2 x^2 + \omega_y^2 y^2 + \omega_z^2 z^2). \tag{5}$$

For an electron confined in a harmonic oscillator potential the Schrödinger equation (1) has a well known analytical solution. The eigenvalues are given by

$$E_0^{\omega} = \omega_x(\nu_x + 1/2) + \omega_y(\nu_y + 1/2) + \omega_z(\nu_z + 1/2). \tag{6}$$

The eigenstates are labelled by a set of three harmonic oscillator quantum numbers (ν_x, ν_y, ν_z). The eigenfunctions are given by a product of three Hermite–Gaussian functions:

$$\chi_{\vec{\nu}}^{\vec{\omega}}(\vec{r}) = N_{\vec{\nu}}^{\vec{\omega}} H_{\nu_x}(x) H_{\nu_y}(y) H_{\nu_z}(z) \exp[-\tfrac{1}{2}(\omega_x x^2 + \omega_y y^2 + \omega_z z^2)], \tag{7}$$

where $N_{\vec{\nu}}^{\vec{\omega}}$ is a normalization constant and $H_{\nu_x}(x)$, etc, stand for a Hermite polynomial. The lowest order Hermite polynomials are

$$H_0(x) = 1, \tag{8}$$

$$H_1(x) = 2x, \tag{9}$$

$$H_2(x) = 4x^2 - 2, \tag{10}$$

$$H_3(x) = 8x^3 - 12x, \tag{11}$$

$$H_4(x) = 16x^4 - 48x^2 + 12. \tag{12}$$

The eigenvalues for an electron confined in a *spherical* harmonic oscillator potential ($\omega_x = \omega_y = \omega_z = \omega$) are given by

$$E_0^{\omega} = \omega(2\nu + \ell + 3/2). \tag{13}$$

The eigenstates are labelled by the principal quantum number ν and the one-electron angular momentum quantum number l with $\nu = 0, 1, 2, \ldots$ and $l = 0, 1, 2, \ldots$ [49]. It is noted that the one-electron orbitals are not ordered in the hydrogen-like, but in the following, sequence:

$$E_0^{\omega}[0\mathrm{s}] = (3/2)\omega, \tag{14}$$

$$E_0^{\omega}[0\mathrm{p}] = (5/2)\omega, \tag{15}$$

$$E_0^{\omega}[0\mathrm{d}] = E_0^{\omega}[1\mathrm{s}] = (7/2)\omega, \tag{16}$$

$$E_0^{\omega}[0\mathrm{f}] = E_0^{\omega}[1\mathrm{p}] = (9/2)\omega, \tag{17}$$

$$E_0^{\omega}[0\mathrm{g}] = E_0^{\omega}[1\mathrm{d}] = E_0^{\omega}[3\mathrm{s}] = (11/2)\omega, \ldots. \tag{18}$$

The consecutive configuration energies $E_0^{\omega}[\nu_1\ell_1\nu_2\ell_2]$ for two non-interacting electrons are

$$E_0^{\omega}[(0\mathrm{s})^2] = 3\omega, \tag{19}$$

$$E_0^{\omega}[0\mathrm{s}0\mathrm{p}] = 4\omega, \tag{20}$$

$$E_0^{\omega}[0\mathrm{s}1\mathrm{s}] = E_0^{\omega}[0\mathrm{s}0\mathrm{d}] = E_0^{\omega}[(0\mathrm{p})^2] = 5\omega, \tag{21}$$

$$E_0^{\omega}[0\mathrm{s}1\mathrm{p}] = E_0^{\omega}[1\mathrm{s}0\mathrm{p}] = E_0^{\omega}[0\mathrm{s}0\mathrm{f}] = E_0^{\omega}[0\mathrm{p}0\mathrm{d}] = 6\omega, \ldots. \tag{22}$$

The degenerate energy levels are split due to the electron interaction. If this splitting is smaller than that due to the Hooke's law potential (i.e. if the separation between the extreme energies

of the terms related to the same configuration is smaller than ω), then the consecutive singlet energies are

$$E^{\omega}[\mathrm{S(0s)}^2] < E^{\omega}[\mathrm{P(0s0p)}] < E^{\omega}[\mathrm{D(0s0d)}] < E^{\omega}[\mathrm{S(0s1s)}] < E^{\omega}[\mathrm{S(0p)}^2] < E^{\omega}[\mathrm{D(0p)}^2] < \cdots. \tag{23}$$

The eigenvalues for an electron confined in an *elliptical* harmonic oscillator potential are given by

$$E_0^{\omega} = \omega(\nu_x + \nu_y + 1) + \omega_z(\nu_z + 1/2). \tag{24}$$

The eigenstates are labelled by a set of three harmonic oscillator quantum numbers (ν_x, ν_y, ν_z), or equivalently by specifying the z component of the one-electron angular momentum quantum numbers as (ν, l_z, ν_z), where $\nu = \nu_x + \nu_y$ and $l_z = \nu, \nu - 2, \ldots, 0$ or 1 for $\nu =$ even or odd. The orbital energies are expressed as a combination of two harmonic oscillator sequences of ω and ω_z, and orbitals belonging to the same (ν, ν_z) manifold with different values of ℓ_z are degenerate. Two different types of elliptical confinement, i.e. prolate type ($\omega_x = \omega_y > \omega_z$) and oblate type ($\omega_x = \omega_y < \omega_z$), have been studied in this contribution. The ratio between the larger ω and the smaller ω has been chosen to be 0.5.

Using the potential defined by equation (5), the total energies of the confined quantum system have been calculated as the eigenvalues of the CI matrix. The one-electron orbitals have been obtained by solving the HF–Roothaan equations. All calculations have been performed using OpenMol [50], an object-oriented programme developed in the Molecular Physics Group of the Max-Planck-Institute for Astrophysics that has been extended to account for power series one-electron potentials and *anisotropic* Gaussian basis functions. The electron density plots have been generated by using the gOpenMol programme[2]. The full CI wavefunction has been used in all calculations.

2.2. Basis-set

It is noted that a quantum chemical standard spherical or Cartesian Gaussian basis set is not the most appropriate choice to expand the eigenfunctions of an electron in an *anisotropic* harmonic oscillator potential given by equation (7). The inspection of the explicit form of the eigenfunctions suggests expanding them in a properly constructed set of *Cartesian anisotropic* Gaussian-type orbitals (c-aniGTO) [51, 52]. The following four types of basis sets have been explored in an attempt to find the most suitable basis set for expanding the eigenfunctions of an electron in an anisotropic harmonic oscillator potential:

- A basis set of *c-aniGTO* with one function for each type of orbital of the following general form:

$$\chi^{\mathrm{c}}_{\mathrm{ani}}(\vec{r}) = x^{a_x} y^{a_y} z^{a_z} \exp(-\zeta_x x^2 - \zeta_y y^2 - \zeta_z z^2). \tag{25}$$

  The orbital exponents are chosen to be $(\zeta_x, \zeta_y, \zeta_z) = (\omega_x/2, \omega_y/2, \omega_z/2)$. Following the quantum-chemical convention, these orbitals are classified as s-, p-, d-type, ... for $a = a_x + a_y + a_z = 0, 1, 2, \ldots$, respectively.
- A basis set of *spherical anisotropic Gaussian-type orbitals (s-aniGTO)* with one function for each type of orbital of the following general form:

$$\chi^{\mathrm{s}}_{\mathrm{ani}}(\vec{r}) = r^l Y_{lm} \exp(-\zeta_x x^2 - \zeta_y y^2 - \zeta_z z^2), \tag{26}$$

  where Y_{lm} is a real spherical harmonic. The product $r^l Y_{lm}$ can be expressed in terms of a sequence of xyz Cartesian coordinates. The orbital exponents are chosen to be

[2] gOpenMol Program; http://www.csc.fi/gopenmol/

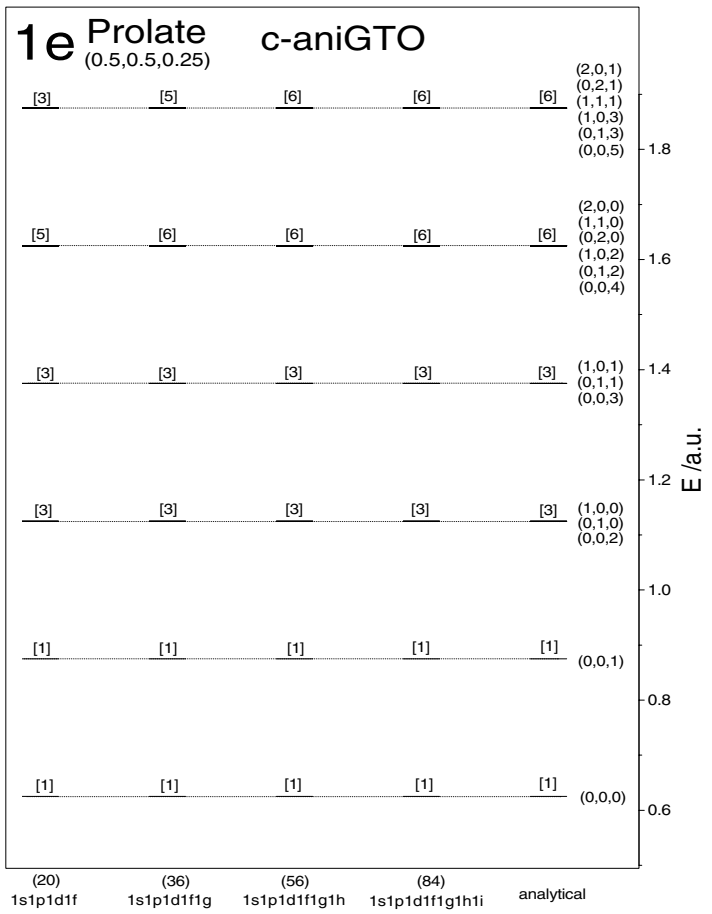

Figure 1. Spectrum of one-electron quantum dot confined by a prolate-type elliptical harmonic oscillator potential with $(\omega_x, \omega_y, \omega_z) = (0.5, 0.5, 0.25)$ for different Cartesian anisotropic Gaussian basis sets. The analytical spectrum labelled by the harmonic oscillator quantum numbers (ν_x, ν_y, ν_z) is shown on the right-hand side. The states are labelled by their degeneracy in square brackets. The total number of basis functions is given in round brackets.

$(\zeta_x, \zeta_y, \zeta_z) = (\omega_x/2, \omega_y/2, \omega_z/2)$. Following the quantum-chemical convention, these orbitals are classified as s-, p-, d-type, ... for $l = 0, 1, 2, \ldots$, respectively.

- A basis set of *s-aniGTO* with a set of functions for each type of orbital.
- A basis set of *conventional spherical Gaussian-type orbitals (s-GTO)*

For the latter two basis sets the orbital exponents have been generated by using the geometrical formula [53]

$$\zeta_{j,\ell} = \alpha_\ell \beta_\ell^{j-1}, \qquad j = 1, 2, \ldots, m_\ell \tag{27}$$

where $\ell = 0, 1, 2, 3, 4, 5, 6$ corresponds, respectively, to s-, p-, d-, f-, g-, h-, i-type basis functions. The minimum and maximum exponents have been chosen dynamically according to the strength of confinement for s-aniGTOs as

$$\zeta_{\mathrm{min},\ell}^{\{x,y,z\}} = \tfrac{1}{2}\omega_{\{x,y,z\}}/c_\ell, \tag{28}$$

$$\zeta_{\mathrm{max},\ell}^{\{x,y,z\}} = c_\ell \times \tfrac{1}{2}\omega_{\{x,y,z\}}, \tag{29}$$

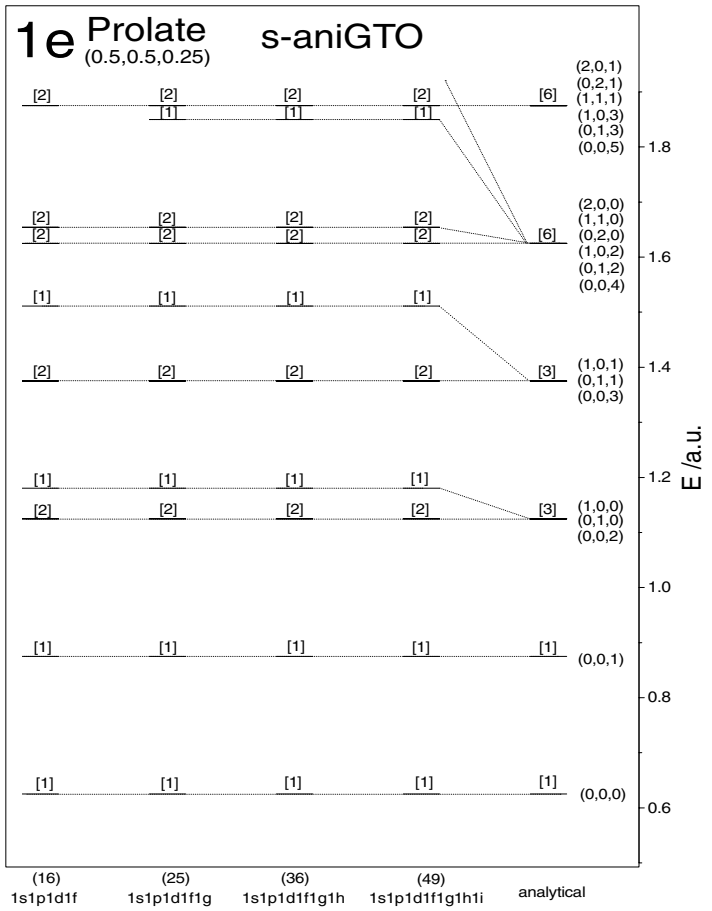

Figure 2. Spectrum of one-electron quantum dot confined by a prolate-type elliptical harmonic oscillator potential with $(\omega_x, \omega_y, \omega_z) = (0.5, 0.5, 0.25)$ for different spherical anisotropic Gaussian basis sets. The analytical spectrum labelled by the harmonic oscillator quantum numbers (ν_x, ν_y, ν_z) is shown on the right-hand side. The states are labelled by their degeneracy in square brackets. The total number of basis functions is given in round brackets.

and for s-GTOs as

$$\zeta_{\min,\ell} = \min(\tfrac{1}{2}\omega_x, \tfrac{1}{2}\omega_y, \tfrac{1}{2}\omega_z)/c_\ell, \tag{30}$$

$$\zeta_{\max,\ell} = c_\ell \times \max(\tfrac{1}{2}\omega_x, \tfrac{1}{2}\omega_y, \tfrac{1}{2}\omega_z), \tag{31}$$

where $c_\ell = 5, 5, 4, 3, 2, 1$ for $\ell = 0, 1, 2, 3, 4, 5$, respectively. The present choice of the minimum and maximum exponents differs slightly from that used in a previous study for two-electron atoms in a spherical harmonic oscillator potential [46].

For different basis sets covering the four types listed above the energy spectrum has been calculated for a prolate *one*-electron quantum dot with the confinement parameters $(\omega_x, \omega_y, \omega_z) = (0.50, 0.50, 0.25)$. The results are displayed in figures 1–4 and are compared with the analytical energy spectrum. From figure 1 it is evident that the single-exponent c-aniGTO basis set properly describes the displayed eigenstates of an electron in an anisotropic harmonic oscillator potential. The energies calculated by using this basis set agree with the analytical values within numerical errors. It is noticed that, for the two smallest basis sets,

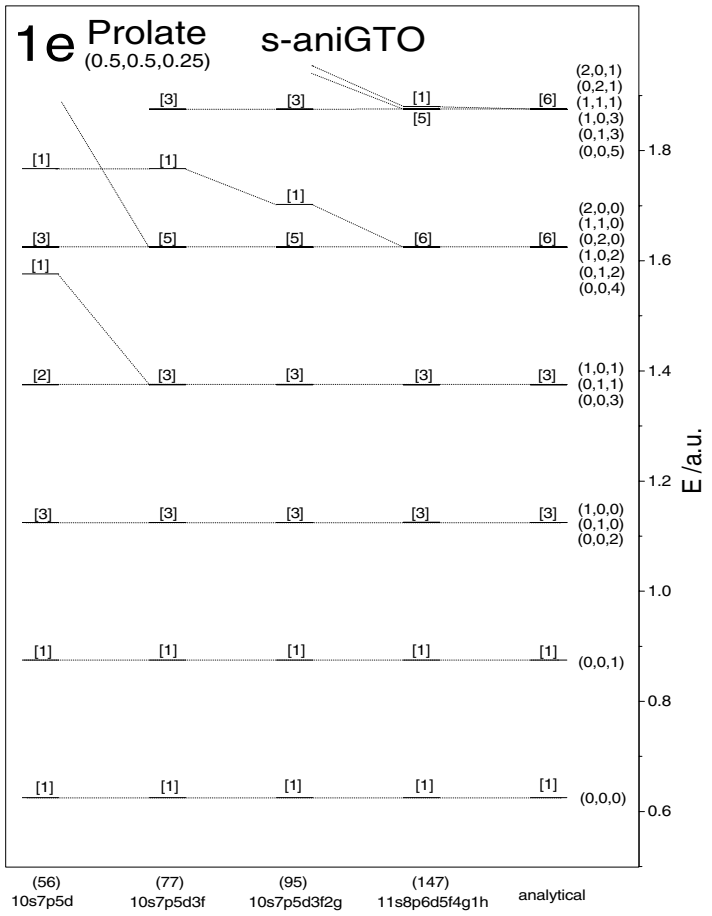

Figure 3. Spectrum of one-electron quantum dot confined by a prolate-type elliptical harmonic oscillator potential with $(\omega_x, \omega_y, \omega_z) = (0.5, 0.5, 0.25)$ for different spherical anisotropic Gaussian basis sets. The analytical spectrum labelled by the harmonic oscillator quantum numbers (ν_x, ν_y, ν_z) is shown on the right-hand side. The states are labelled by their degeneracy in square brackets. The total number of basis functions is given in round brackets.

some of the displayed higher states are absent (compare the numbers in brackets). This is to be expected because these basis sets cannot describe the higher Hermite functions representing the corresponding eigenfunctions. The energy spectrum of a one-electron quantum dot calculated by using a basis set of *single*-exponent s-aniGTOs is presented in figure 2. It demonstrates that the *single*-exponent s-aniGTO basis set describes correctly only part of the eigenstates of an electron in an anisotropic harmonic oscillator potential while others are either completely absent or not described correctly. It is noticed that a state, once present, does not change its value with increasing basis set size. Again, this is expected for this single-exponent basis set because the spherical harmonics present in these basis sets cannot or not fully describe the corresponding Hermite functions. From figure 3 it is seen that the largest *multiple*-exponent s-aniGTO basis set correctly describes the energy spectrum except for one of the highest states studied. While for the *single*-exponent s-aniGTO basis set a state, once it is present, does not change its value, it converges in the present case to the analytical value with increasing basis set size with an accuracy $\delta E < 1.0 \times 10^{-4}$. The energy spectra of an electron in an

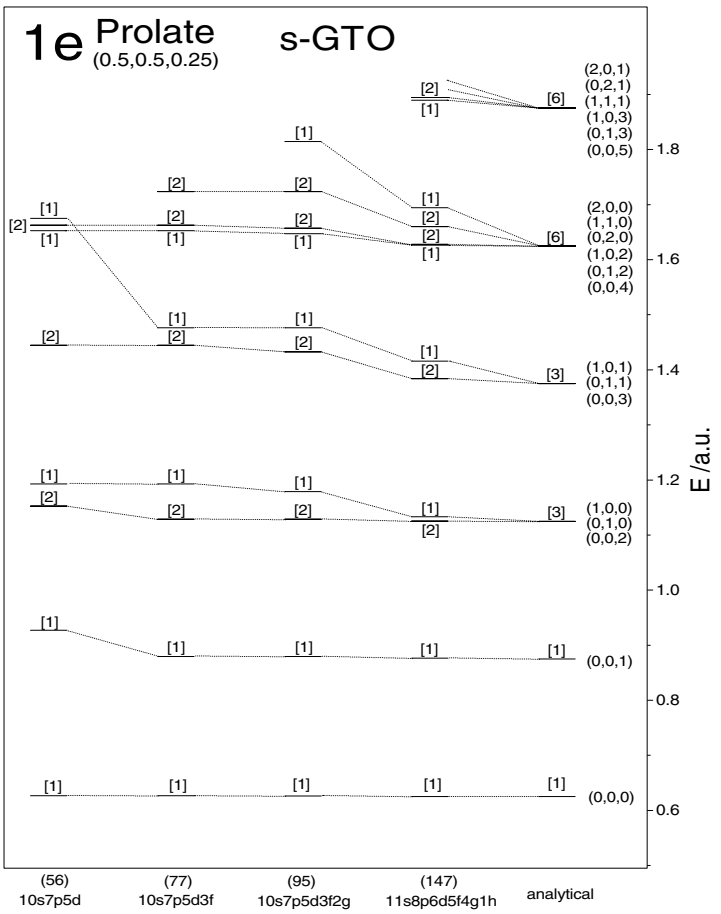

Figure 4. Spectrum of one-electron quantum dot confined by a prolate-type elliptical harmonic oscillator potential with $(\omega_x, \omega_y, \omega_z) = (0.5, 0.5, 0.25)$ for different conventional spherical Gaussian basis sets. The analytical spectrum labelled by the harmonic oscillator quantum numbers (ν_x, ν_y, ν_z) is shown on the right-hand side. The states are labelled by their degeneracy in square brackets. The total number of basis functions is given in round brackets.

anisotropic elliptical harmonic oscillator potential calculated by using a standard quantum chemical standard basis set are shown in figure 4. The results displayed clearly demonstrate that even the largest basis set of 147 functions containing up to h-type orbitals cannot describe correctly the energy spectrum. The eigenstates calculated by using this large basis set are shifted and split increasingly for higher lying states. The results become even worse for an elliptical potential with larger anisotropy.

The energy spectra of a prolate *two*-electron quantum dot with the same confinement parameters as in the one-electron case are displayed for different size single-exponent c-aniGTO basis sets, the largest multiple-exponent s-aniGTO basis set and the largest s-GTO basis set in figure 5. The results presented show that the energy spectra calculated by using the c-aniGTO basis sets converge for increasing size of the basis set and that the energy spectrum calculated by the largest c-aniGTO basis set of 84 functions is almost identical to that calculated by using the largest s-aniGTO basis set, having 147 functions. This again demonstrates that conventional s-GTO basis sets cannot approximate correctly the electronic wavefunction of

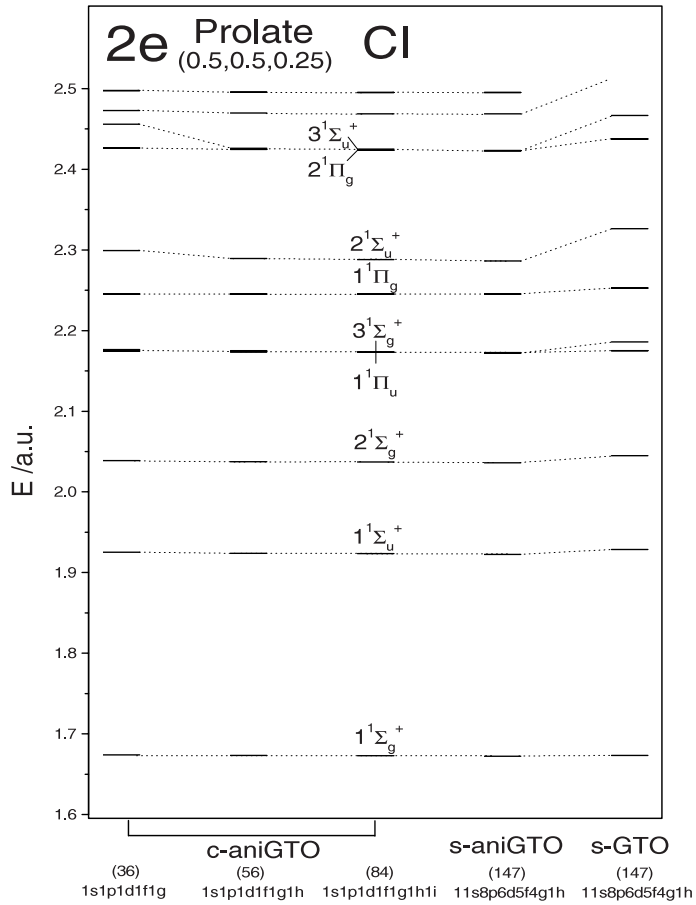

Figure 5. Spectrum of two electrons confined by a prolate-type elliptical harmonic oscillator potential with $(\omega_x, \omega_y, \omega_z) = (0.5, 0.5, 0.25)$ for different basis sets. The total number of basis functions is given in round brackets.

quantum systems in anisotropic harmonic oscillator potentials. Throughout the present study the single-exponent c-aniGTO basis set of 84 functions has been used.

3. Results and discussion

3.1. Hartree–Fock orbitals

The closed-shell HF orbitals for two electrons confined by a spherical harmonic oscillator potential, i.e. for a spherical quantum dot, with the confinement parameters $(\omega_x, \omega_y, \omega_z) = (0.25, 0.25, 0.25)$ are shown in figure 6. The density distribution is displayed in cubes with a side length of 16 au. The z axis is directed along the vertical edge of the cube. The electron density at the surface is 1.0×10^{-4}. The orbitals are labelled by their quantum numbers ν and ℓ defined previously, with the difference that $\nu' = \nu + 1$ has been used to label the states with the one-electron principal quantum numbers $\nu = 0, 1, 2, \ldots$. The HF orbitals are displayed upwards in increasing order of orbital energy. It is noticed that the order differs from that of the hydrogen-like sequence and that the 2s and 1d HF orbitals are not energetically degenerate

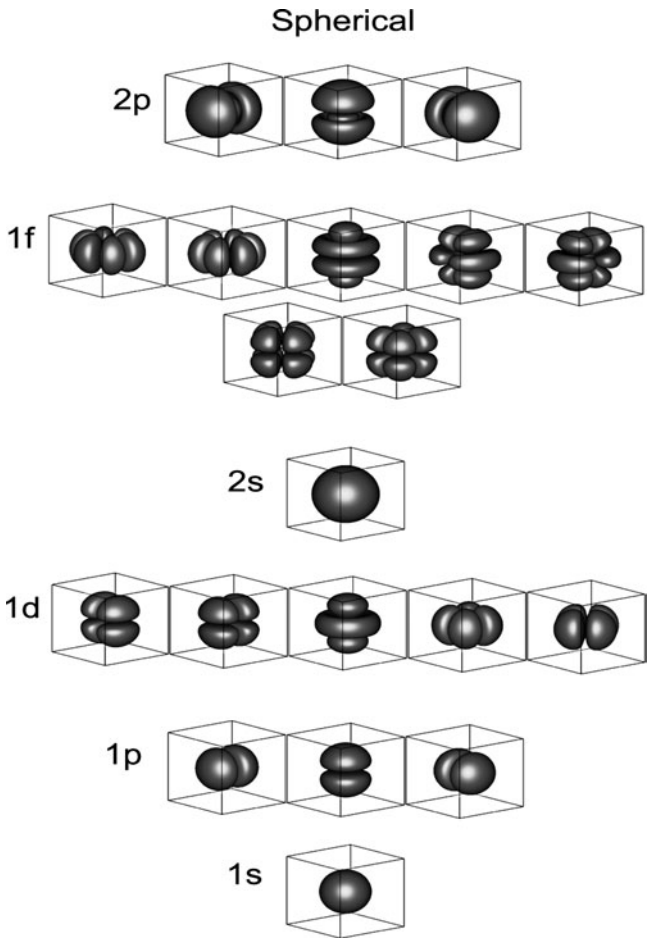

Figure 6. HF orbital density distribution for two electrons confined by a spherical harmonic oscillator potential with $(\omega_x, \omega_y, \omega_z) = (0.25, 0.25, 0.25)$. The 1s orbital is occupied, while the other orbitals are virtual. The density at the surface shown is 1.0×10^{-4}.

as the eigenfunctions of an electron in an isotropic harmonic oscillator potential. The orbitals show the same shape as the hydrogen-like orbitals with the same angular momentum quantum numbers.

The HF orbitals for a prolate and an oblate quantum dot are displayed in figure 7. The confinement parameters are (0.5, 0.5, 0.25) and (0.25, 0.25, 0.5), respectively. The notation $[\nu, \nu_z]\Delta$ is used for labelling the one-electron orbitals, where ν and ν_z are the quantum numbers defined previously and Δ represents a symmetry label of the $D_{\infty h}$ symmetry group. It is noted that, for the prolate quantum dot, the following three groups of orbitals (i) $[0, 2]\sigma_g$ and $[1, 0]\pi_u$, (ii) $[0, 3]\sigma_u$ and $[1, 1]\pi_g$, (iii) $[0, 4]\sigma_g$, $[1, 2]\pi_u$, $[2, 0]\delta_g$ and $[2, 0]\sigma_g$, which are energetically degenerate for the one-electron quantum dot, are not degenerate in the HF approximation due to the presence of electron–electron interactions. Similarly, for the oblate quantum dot the two groups of orbitals (i) $[2, 0]\delta_g$, $[2, 0]\sigma_g$, and $[0, 1]\sigma_u$ and (ii) $[3, 0]\phi_u$, $[3, 0]\pi_u$ and $[1, 1]\pi_g$ are not degenerate in the HF approximation. An inspection of figure 7 reveals several interesting features: the orbitals of the prolate quantum dot are stretched along the z axis, while those of the oblate quantum dot are compressed with respect to this axis, as is to be expected.

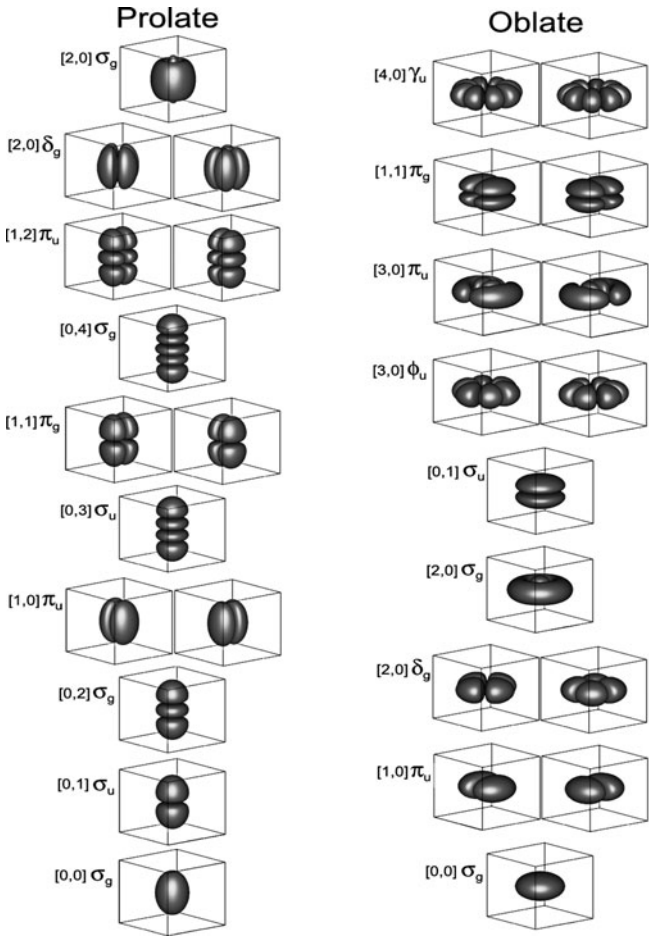

Figure 7. HF orbital density distribution for two electrons confined by a prolate-type and an oblate-type elliptical harmonic oscillator potential with $(\omega_x, \omega_y, \omega_z) = (0.5, 0.5, 0.25)$ and $(0.25, 0.25, 0.5)$, respectively. The $[0, 0]\sigma_g$ orbital is occupied, while the other orbitals are virtual. The density at the surface shown is 1.0×10^{-4}.

The nodal planes of the orbitals of the prolate quantum dot tend to be aligned in the xy plane while those of the oblate quantum dot tend to be aligned in the xz and yz planes, respectively. These observations are confirmed by the angular momentum quantum numbers of the orbitals. The highest angular momentum quantum number among the 10 lowest orbitals of the prolate quantum dot is $l = 2$ (δ state), while that for the oblate quantum dot is as large as $l = 4$ (γ state). The relation between the labels of the orbitals and the number of nodal planes is as follows: the number of horizontal nodal planes is equal to the ν_z quantum number, while the number of vertical nodal planes is equal to the ν quantum number except for the $[2, 0]\sigma_g$ state having a 'circular node' with respect to the z axis.

The correspondence between the HF orbitals of the spherical, prolate and oblate quantum dots is shown in figure 8. The 1s orbital of the spherical quantum dot corresponds to the $[0, 0]\sigma_g$ orbital of both the prolate and the oblate quantum dot. The $[0, 0]\sigma_g$ orbital of the prolate quantum dot is extended along the z axis and the orbital of the oblate quantum dot is compressed with respect to it. The triply degenerate 1p orbitals of the spherical quantum

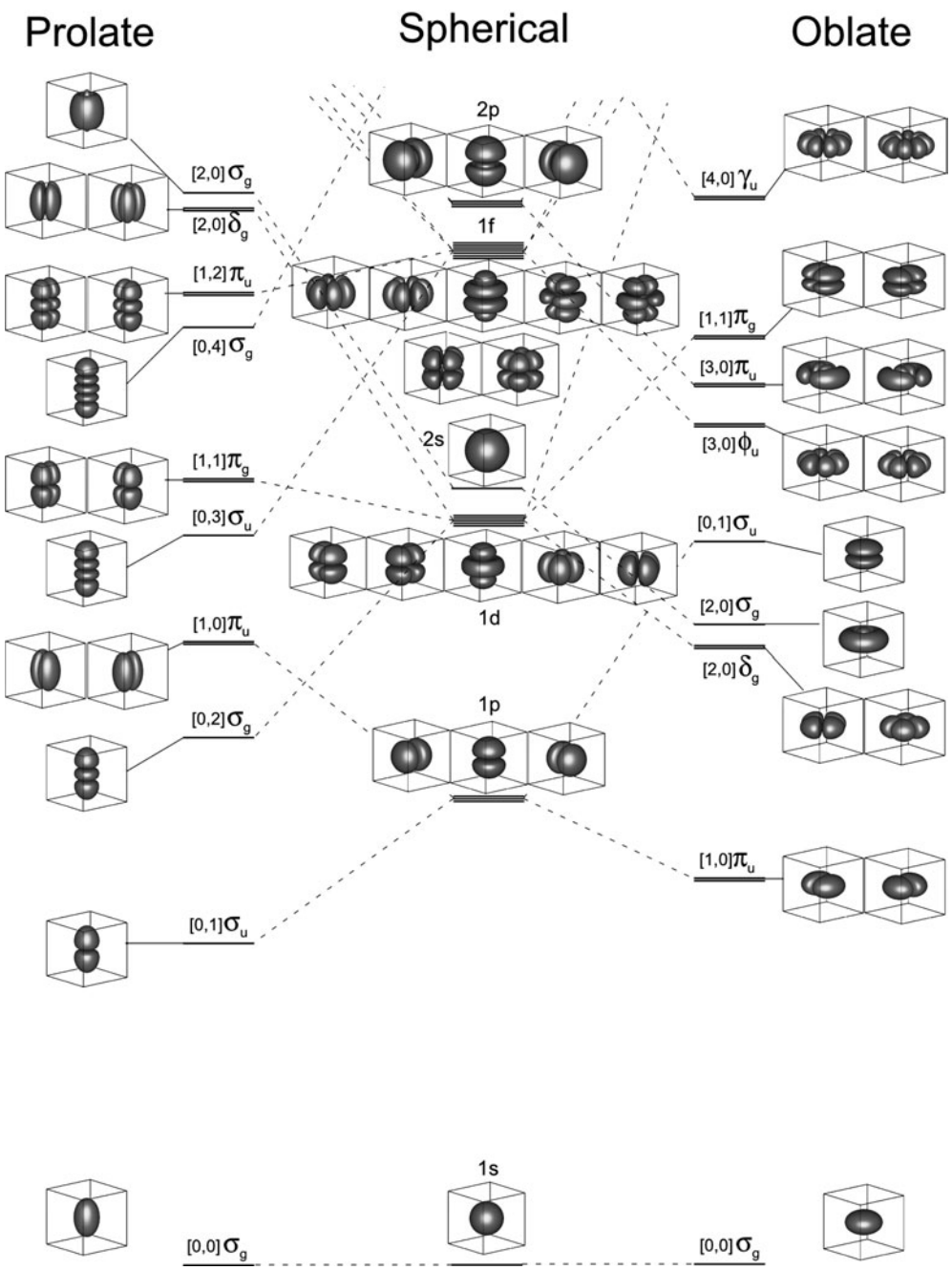

Figure 8. Correspondence between the HF orbitals of a spherical, a prolate and an oblate quantum dot.

dot correspond to the $[0, 1]\sigma_u$ orbital and the doubly degenerate $[1, 0]\pi_u$ orbitals of both the prolate and the oblate quantum dot. However, while the $[0, 1]\sigma_u$ orbital has a lower orbital energy than the $[1, 0]\pi_u$ orbital in the case of the prolate quantum dot, the order is reversed for

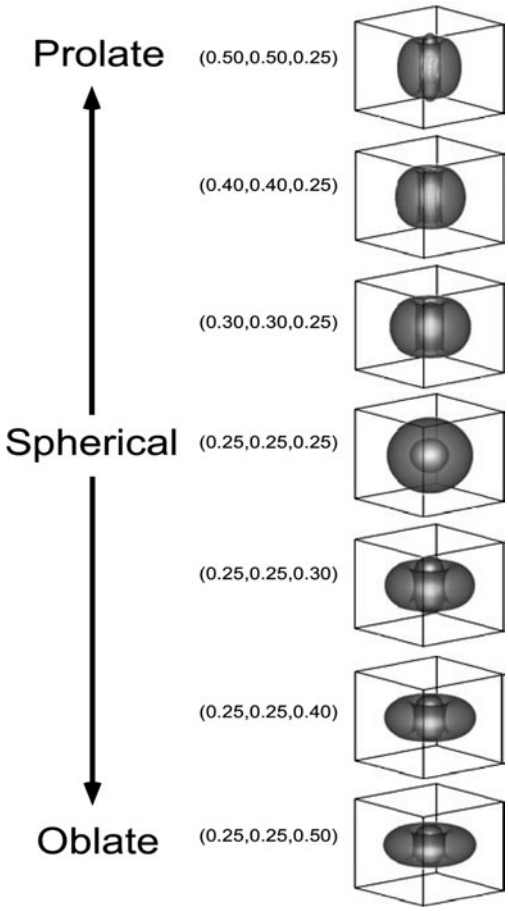

Figure 9. Correspondence between the HF orbitals of a spherical, a prolate and an oblate quantum dot.

the oblate quantum dot. Correspondingly, the 1d orbitals of the spherical quantum dot are split into three sets of orbitals, $[0, 2]\sigma_g$, $[1, 1]\pi_g$ and $[2, 0]\delta_g$ for the prolate and oblate quantum dot, the 1f orbitals are split into four sets, and so on.

The correspondence between the topological structure of the spherical-, prolate- and oblate-type HF orbitals and the number of nodal planes shows some interesting features: for 1ℓ ($\ell = \mathrm{s, p, d, f}$) orbitals with no radial node, the spherical orbitals transform into prolate- and oblate-type orbitals, respectively, by preserving the number of horizontal and vertical nodal planes. For example, the $1d_{3z^2-r^2}$ spherical orbital that has two horizontal nodal planes and no vertical nodal plane corresponds to the $[0, 2]\sigma_g$ orbital of the prolate quantum dot that has the same number of horizontal and vertical nodal planes, and the $1d_{xy}$ and $1d_{x^2-y^2}$ orbitals that have two vertical and no horizontal nodal planes correspond to the $[2, 0]\delta_g$ orbitals of the oblate quantum dot that have the same number and type of nodal planes. The corresponding relation between orbitals that have radial nodes is more complex. The correspondence of the 2s orbital to the $[2, 0]\sigma_g$ orbital of the prolate and oblate quantum dot, respectively, is displayed in figure 9. It is noted that the radial node of the orbital is deformed vertically, resulting in a circular node around the z axis as the spherical confining potential is changed to a prolate-type and an oblate-type elliptical potential.

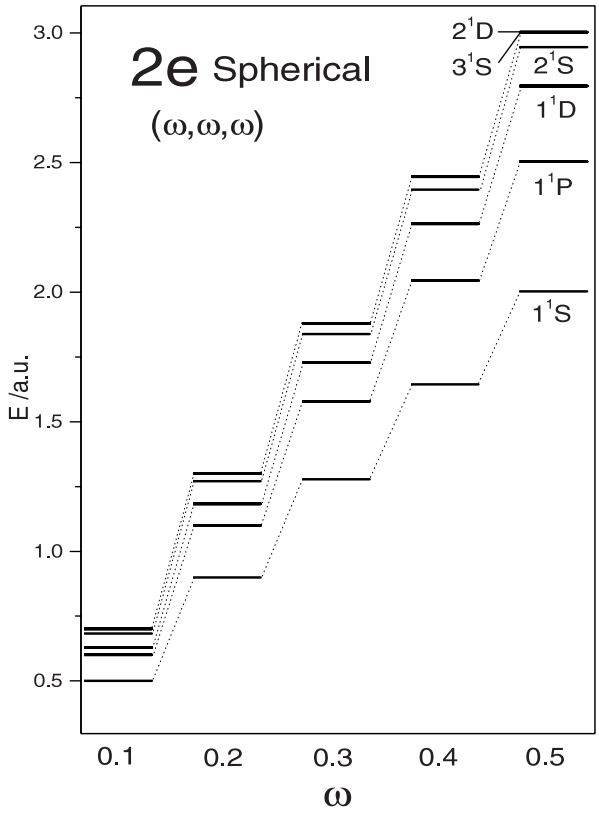

Figure 10. Spectra of two electrons confined by a spherical harmonic oscillator potential with $\omega = 0.1$, 0.2, 0.3, 0.4, and 0.5.

3.2. Energy spectra and electron-density distributions

3.2.1. Spherical quantum dots. The energy spectra for the lowest six singlet states of two electrons confined by a spherical potential with different values of $(\omega_x, \omega_y, \omega_z) = (\omega, \omega, \omega)$, $0.0 \leqslant \omega \leqslant 0.5$, are displayed in figure 10. It is noted that the absolute energies and the spacing between adjacent energy levels increases as the strength of the confinement ω increases. This is expected, of course, from a simple *particle in a box model*. The lowest six states are $1\,^1$S, $1\,^1$P, $1\,^1$D, $2\,^1$S, $3\,^1$S and $2\,^1$D, where the first number counts the states, separately for each symmetry, in increasing order of energy. The sequence of the lowest four states is the same as that of the orbital energies, i.e. 1s < 1p < 1d < 2s, as shown in figure 8, but this is not true for the higher states.

The two leading configurations and their contributions to the CI wavefunction of the lowest six singlet states confined by a spherical potential with $\omega = 0.5$ are listed in table 1. The CI wavefunction of the lowest two states, $1\,^1$S and $1\,^1$P, is completely dominated by one configuration, namely $(1s)^2$ and (1s)(1p), respectively. On the other hand, the CI wavefunction of the four other states, $1\,^1$D, $2\,^1$S, $3\,^1$S and $2\,^1$D, is dominated by two configurations. The $(1p)^2$ configuration gives rise to one S and one D state, each of which interacts with the S state of $(1s)^2$ configuration and the D state of (1s)(1d) configuration, respectively, resulting in two S states ($2\,^1$S and $3\,^1$S) and two D states ($1\,^1$D and $2\,^1$D). This large configuration mixing may be ascribed to the fact that the excitation energy from the lowest 1s orbital to the 1d and 2s orbitals, 1.214 and 1.251, respectively, is close to twice that of the 1p orbital of 0.766.

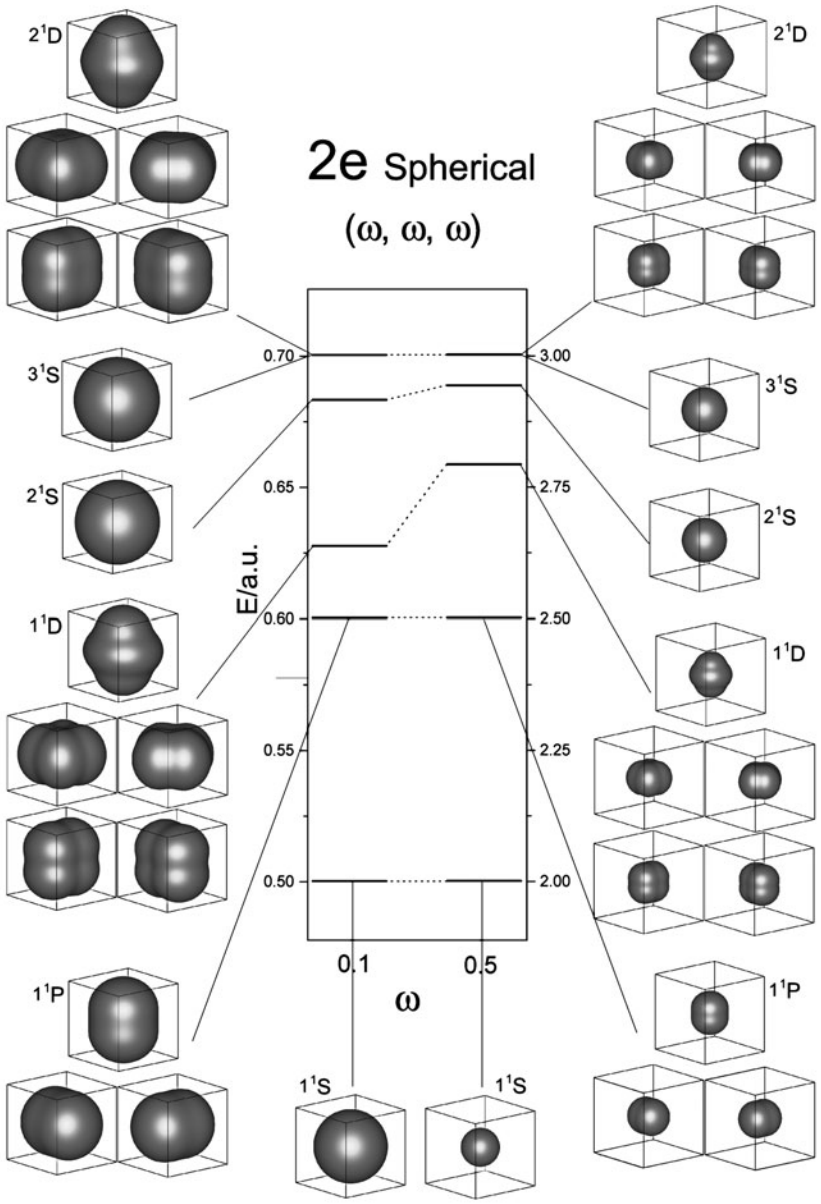

Figure 11. Electron-density distribution and energy diagram for two electrons confined by a spherical harmonic oscillator potential with $\omega = 0.1$ (left) and 0.5 (right). The density at the surface shown is 1.0×10^{-4}.

The electron-density distribution of two electrons confined by a spherical potential with $\omega = 0.1$ and 0.5 is shown in figure 11 together with the diagram of the corresponding CI energies. The electron-density distribution is displayed in the same way as for the HF orbitals. The axes of the energy diagram are scaled such the lowest and the highest states are on the same level for $\omega = 0.1$ and 0.5. The most striking observation is the compressed electron density distribution for $\omega = 0.5$ as compared to that for $\omega = 0.1$. Another interesting feature

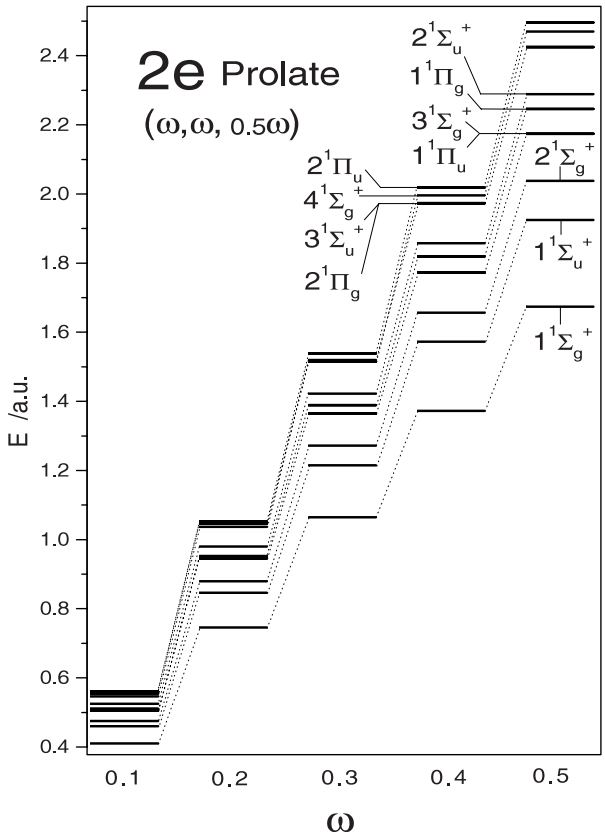

Figure 12. Spectrum of two electrons confined by a prolate-type elliptical harmonic oscillator potential with $\omega = 0.1$, 0.2, 0.3, 0.4 and 0.5.

Table 1. The two leading configurations and the squared norms of the lowest six singlet states of two electrons confined by a spherical harmonic oscillator potential with $\omega = 0.5$.

State	First configuration	First norm	Second configuration	Second norm
$1\,^1$S	$(1s)^2$	0.974	$(1p)^2$	0.024
$1\,^1$P	(1s)(1p)	0.966	(1p)(1d)	0.022
$1\,^1$D	(1s)(1d)	0.491	$(1p)^2$	0.488
$2\,^1$S	$(1p)^2$	0.487	(1s)(2s)	0.485
$3\,^1$S	(1s)(2s)	0.491	$(1p)^2$	0.444
$2\,^1$D	(1s)(1d)	0.480	$(1p)^2$	0.477

observed immediately is the blurred nodal structure of the density distributions. A comparison of the energy-level structure for $\omega = 0.5$ to that for $\omega = 0.1$ reveals that the energy-level structure is not scalable with ω while for the one-electron quantum dot it scales exactly with ω, as will be discussed later.

3.2.2. Prolate quantum dots. The energy spectra of the low lying singlet states of two electrons confined by a prolate-type elliptical potential with $(\omega_x, \omega_y, \omega_z) = (\omega, \omega, 0.5 \times \omega)$, $0.1 \leqslant \omega \leqslant 0.5$, are shown in figure 12. The electron density distribution of these states

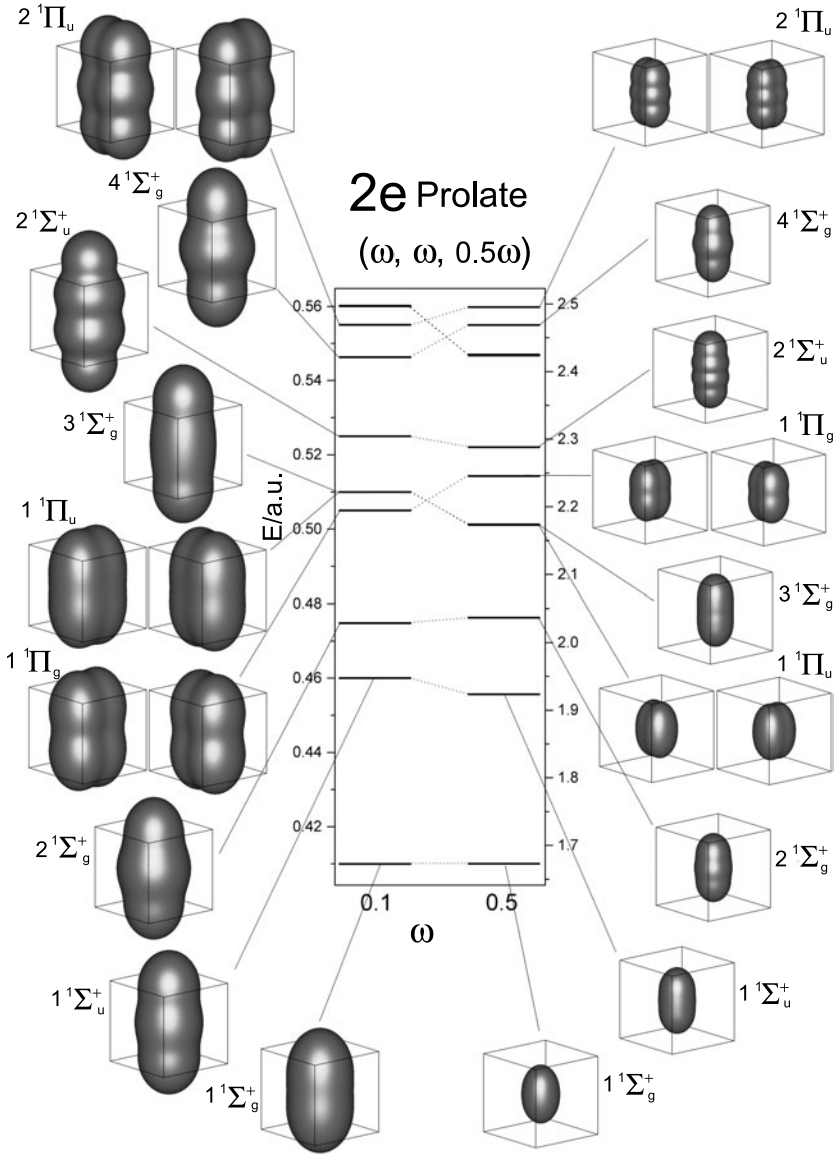

Figure 13. Electron-density distribution for two electrons confined by a prolate-type elliptical harmonic oscillator potential with $\omega = 0.1$ (left) and 0.5 (right). The density at the surface shown is 1.0×10^{-4}.

for $\omega = 0.1$ and 0.5 and the corresponding energy diagram are displayed in figure 13. As observed already in the case of the spherical quantum dot the energies and the spacing between adjacent levels increase as ω increases. Similarly, as in the spherical case, no scalability of the CI energies with ω is observed. However, in the case of the prolate quantum dot, the order of the energy levels as well as the ratio of the spacings between energy levels differs between $\omega = 0.1$ and 0.5. For example, for $\omega = 0.1$ the fourth to sixth levels in increasing order of CI energy are $1\ ^1\Pi_g < 1\ ^1\Pi_u < 3\ ^1\Sigma_g^+$, while those for $\omega = 0.5$ are $1\ ^1\Pi_u < 3\ ^1\Sigma_g^+ < 1\ ^1\Pi_g$. A reversed order of energy levels is also observed for the eighth to the eleventh levels.

Table 2. The two leading configurations and their squared norms for the lowest seven singlet states of two electrons confined by a prolate-type elliptical harmonic oscillator potential with $(\omega_x, \omega_y, \omega_z) = (0.5, 0.5, 0.25)$ and $(0.1, 0.1, 0.05)$.

State	First configuration	First norm	Second configuration	Second norm
		$\omega = 0.5$		
$1\,^1\Sigma_g^+$	$([0,0]\sigma_g)^2$	0.942	$([0,1]\sigma_u)^2$	0.037
$1\,^1\Sigma_u^+$	$([0,0]\sigma_g)([0,1]\sigma_u)$	0.910	$([0,1]\sigma_u)([0,2]\sigma_g)$	0.067
$2\,^1\Sigma_g^+$	$([0,0]\sigma_g)([0,2]\sigma_g)$	0.489	$([0,1]\sigma_u)^2$	0.446
$1\,^1\Pi_u$	$([0,0]\sigma_g)([1,0]\pi_u)$	0.937	$([0,1]\sigma_u)([1,1]\pi_g)$	0.038
$3\,^1\Sigma_g^+$	$([0,0]\sigma_g)([0,2]\sigma_g)$	0.446	$([0,1]\sigma_u)^2$	0.399
$1\,^1\Pi_g$	$([0,0]\sigma_g)([1,1]\pi_g)$	0.482	$([0,1]\sigma_u)([1,0]\pi_u)$	0.477
$2\,^1\Sigma_u^+$	$([0,0]\sigma_g)([0,3]\sigma_u)$	0.729	$([0,1]\sigma_u)([0,2]\sigma_g)$	0.200
		$\omega = 0.1$		
$1\,^1\Sigma_g^+$	$([0,0]\sigma_g)^2$	0.778	$([0,1]\sigma_u)^2$	0.128
$1\,^1\Sigma_u^+$	$([0,0]\sigma_g)([0,1]\sigma_u)$	0.683	$([0,1]\sigma_u)([0,2]\sigma_g)$	0.199
$2\,^1\Sigma_g^+$	$([0,0]\sigma_g)([0,2]\sigma_g)$	0.459	$([0,1]\sigma_u)^2$	0.311
$1\,^1\Pi_g$	$([0,0]\sigma_g)([1,1]\pi_g)$	0.428	$([0,1]\sigma_u)([1,0]\pi_u)$	0.411
$1\,^1\Pi_u$	$([0,0]\sigma_g)([1,0]\pi_u)$	0.762	$([0,1]\sigma_u)([1,1]\pi_g)$	0.126
$3\,^1\Sigma_g^+$	$([0,0]\sigma_g)([0,2]\sigma_g)$	0.323	$([0,1]\sigma_u)^2$	0.196
$2\,^1\Sigma_u^+$	$([0,0]\sigma_g)([0,3]\sigma_u)$	0.697	$([0,1]\sigma_u)([0,2]\sigma_g)$	0.089

Again, the most striking observation from figure 13 is the compressed density distribution for $\omega = 0.5$ (right-hand side) as compared to those for $\omega = 0.1$ (left-hand side). The shape of the electron distributions of corresponding states for both values of ω are similar except that the surface of the $1\,^1\Sigma_g^+$ and the $1\,^1\Sigma_u^+$ states for $\omega = 0.1$ show a weak nodal pattern while those for $\omega = 0.5$ do not. The two leading configurations and their contribution to the CI wavefunction of the lowest seven singlet states both for $\omega = 0.1$ and 0.5 are listed in table 2. The CI wavefunction of the ground $1\,^1\Sigma_g^+$ state, the first excited $1\,^1\Sigma_u^+$ state and the fourth $1\,^1\Pi_u$ state for $\omega = 0.5$ are completely dominated by one configuration with a squared norm larger than 0.9, namely $([0,0]\sigma_g)^2$, $([0,0]\sigma_g)([0,1]\sigma_u)$ and $([0,0]\sigma_g)([1,0]\pi_u)$, respectively. On the other hand, the same states for $\omega = 0.1$ have non-negligible contributions from a second configuration. It would be interesting to address the relation between the weak nodal pattern observed for $\omega = 0.1$ for the density surfaces of the $1\,^1\Sigma_g^+$ and the $1\,^1\Sigma_u^+$ state and their second leading configuration. The electron-density surface of the $1\,^1\Sigma_g^+$ state for $\omega = 0.1$ has a weak node around its centre, although the HF orbital of the first configuration $[0,0]\sigma_g$ has no node, as seen from figure 7. On the other hand, the HF orbital of the second leading configuration of this state, $[0,1]\sigma_u$, has a node around its centre, as shown in the same figure. A similar relation could be seen between the nodal pattern of the electron-density surface and the orbital of the second leading configuration of the $1\,^1\Sigma_u^+$ state for $\omega = 0.1$.

3.2.3. Oblate quantum dots. The energy spectra for the lowest nine singlet states of two electrons confined by an oblate-type elliptical potential with $(\omega_x, \omega_y, \omega_z) = (0.5 \times \omega, 0.5 \times \omega, \omega)$, $0.1 \leqslant \omega \leqslant 0.5$ are displayed in figure 14. The spectra show a behaviour similar to that observed for the spherical and the prolate quantum dots: the energies and the spacing between energy levels increase with increasing strength of the confinement. The electron-density distributions for $\omega = 0.1$ and 0.5 and the corresponding energy diagram are displayed in figure 15. Again, the electron-density distribution for $\omega = 0.5$ is strongly compressed as

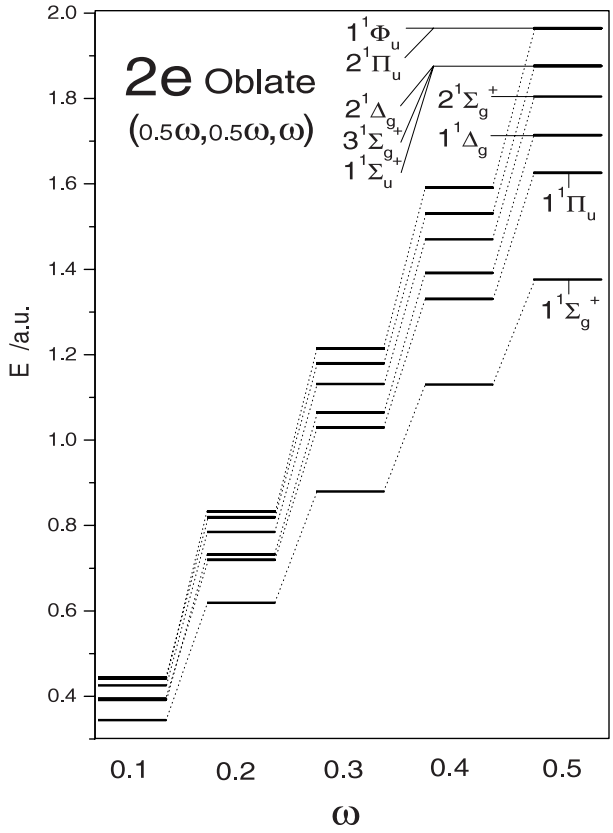

Figure 14. Spectrum of two electrons confined by an oblate-type elliptical harmonic oscillator potential with $\omega = 0.1$, 0.2, 0.3 0.4 and 0.5.

compared to that for $\omega = 0.1$, as observed previously. The shape of all electron-density surfaces displayed are compressed with respect to the z axis, as observed for the corresponding HF orbitals shown in figures 7 and 8, but only small remnants of the nodal structure can be observed.

As found previously for spherical and prolate quantum dots the energy-level structure does not scale with ω. Already the ordering of the first and second excited states reverses between $\omega = 0.1$ and 0.5. The ordering of the energy levels changes in a complicated way for the fifth to eighth level between $\omega = 0.1$ and 0.5. The two leading configurations and their contributions to the CI wavefunction of the lowest nine singlet states for $\omega = 0.1$ and 0.5 are listed in table 3. The CI wavefunction of the ground $1\ ^1\Sigma_g^+$ state and the first excited $1\ ^1\Pi_u$ state for $\omega = 0.5$ is dominated by a single configuration with a squared norm larger than 0.9, namely $([0, 0]\sigma_g)^2$ and $([0, 0]\sigma_g)([1, 0]\pi_u)$, respectively. On the other hand, the same states for $\omega = 0.1$ have non-negligible contributions from a second configuration. The list of configurations in table 3 shows that the $([1, 0]\pi_u)^2$ configuration plays an important role in the four states, $1\ ^1\Delta_g$, $2\ ^1\Sigma_g^+$, $2\ ^1\Delta_g$ and $3\ ^1\Sigma_g^+$. The $([1, 0]\pi_u)^2$ configuration gives rise to one Σ_g state and one Δ_g state, each of which may interact with the Σ_g state originating from the configuration $([0, 0]\sigma_g)([2, 0]\sigma_g)$ and with the Δ_g state originating from the configuration $([0, 0]\sigma_g)([2, 0]\delta_g)$, respectively, resulting in two Σ_g states ($2\ ^1\Sigma_g^+$ and $3\ ^1\Sigma_g^+$) and two Δ_g states ($1\ ^1\Delta_g$ and $2\ ^1\Delta_g$). This configuration mixing may be ascribed to the fact that the excitation

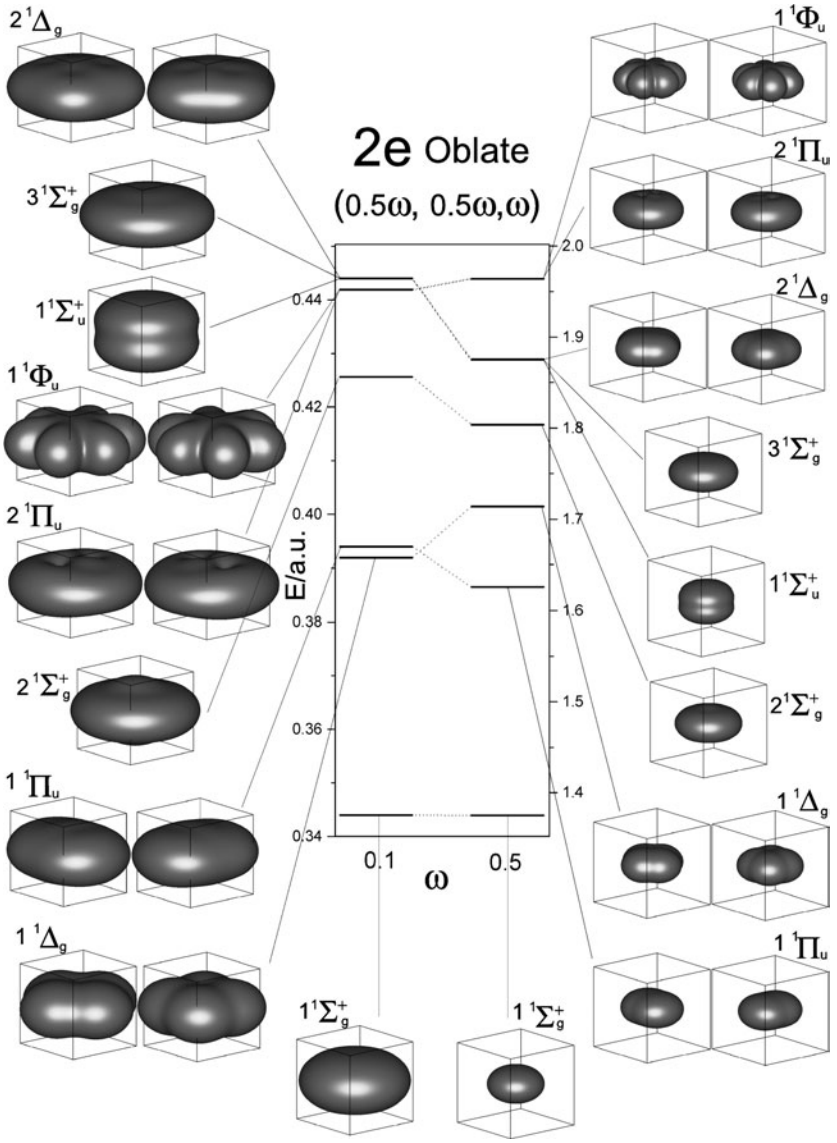

Figure 15. Electron-density distribution for two electrons confined by an oblate-type elliptical harmonic oscillator potential with $\omega = 0.1$ (left) and 0.5 (right). The density at the surface shown is 1.0×10^{-4}.

energies from the lowest $[0, 0]\sigma_g$ one-electron state to the $[2, 0]\delta_g$ and $[2, 0]\sigma_g$ states of 0.645 and 0.667, respectively, are close to twice that of the $[1, 0]\pi_u$ state. The leading configurations of these four states for $\omega = 0.1$ are the same as those for $\omega = 0.5$.

3.3. Scalability and electron correlation

It has been observed that the energy-level structure for all three types of two-electron quantum dots for different ω does not scale with ω. However, in the case of one-electron quantum dots the energy-level structure for ω_1 and ω_2 scales as ω_1/ω_2. As expected, the non-scalability

Table 3. The two leading configurations and their squared norms for the lowest nine singlet states of two electrons confined by an oblate-type elliptical harmonic oscillator potential with $(\omega_x, \omega_y, \omega_z) = (0.25, 0.25, 0.5)$ and $(0.05, 0.05, 0.1)$

State	First configuration	First norm	Second configuration	Second norm
		$\omega = 0.5$		
$1\,^1\Sigma_g^+$	$([0,0]\sigma_g)^2$	0.946	$([1,0]\pi_u)^2$	0.038
$1\,^1\Pi_u$	$([0,0]\sigma_g)([1,0]\pi_u)$	0.925	$([1,0]\pi_u)([2,0]\delta_g)$	0.039
$1\,^1\Delta_g$	$([0,0]\sigma_g)([2,0]\delta_g)$	0.483	$([1,0]\pi_u)^2$	0.474
$2\,^1\Sigma_g^+$	$([0,0]\sigma_g)([2,0]\sigma_g)$	0.487	$([1,0]\pi_u)^2$	0.457
$1\,^1\Sigma_u^+$	$([0,0]\sigma_g)([0,1]\sigma_u)$	0.941	$([1,0]\pi_u)([1,1]\pi_g)$	0.038
$3\,^1\Sigma_g^+$	$([0,0]\sigma_g)([2,0]\sigma_g)$	0.461	$([1,0]\pi_u)^2$	0.402
$2\,^1\Delta_g$	$([0,0]\sigma_g)([2,0]\delta_g)$	0.453	$([1,0]\pi_u)^2$	0.449
$2\,^1\Pi_u$	$([1,0]\pi_u)([2,0]\sigma_g)$	0.469	$([0,0]\sigma_g)([3,0]\pi_u)$	0.240
$1\,^1\Phi_u$	$([0,0]\sigma_g)([3,0]\phi_u)$	0.724	$([1,0]\pi_u)([2,0]\delta_g)$	0.235
		$\omega = 0.1$		
$1\,^1\Sigma_g^+$	$([0,0]\sigma_g)^2$	0.829	$([1,0]\pi_u)^2$	0.107
$1\,^1\Delta_g$	$([0,0]\sigma_g)([2,0]\delta_g)$	0.435	$([1,0]\pi_u)^2$	0.406
$1\,^1\Pi_u$	$([0,0]\sigma_g)([1,0]\pi_u)$	0.761	$([1,0]\pi_u)([2,0]\delta_g)$	0.105
$2\,^1\Sigma_g^+$	$([0,0]\sigma_g)([2,0]\sigma_g)$	0.460	$([1,0]\pi_u)^2$	0.360
$2\,^1\Pi_u$	$([1,0]\pi_u)([2,0]\sigma_g)$	0.385	$([0,0]\sigma_g)([3,0]\pi_u)$	0.227
$1\,^1\Phi_u$	$([0,0]\sigma_g)([3,0]\phi_u)$	0.664	$([1,0]\pi_u)([2,0]\delta_g)$	0.194
$1\,^1\Sigma_u^+$	$([0,0]\sigma_g)([0,1]\sigma_u)$	0.804	$([1,0]\pi_u)([1,1]\pi_g)$	0.106
$3\,^1\Sigma_g^+$	$([0,0]\sigma_g)([2,0]\sigma_g)$	0.362	$([1,0]\pi_u)^2$	0.227
$2\,^1\Delta_g$	$([0,0]\sigma_g)([2,0]\delta_g)$	0.350	$([1,0]\pi_u)^2$	0.341

of the spectrum of two-electron quantum dots with ω originates from the electron–electron interaction.

The correlation energy and its percentage of the total CI energy as a function of ω for a spherical, a prolate and an oblate quantum dot are displayed in figure 16. The correlation energy for the free helium atom is shown for comparison. The correlation energy is defined as the difference between the HF and the CI energy. This figure shows some interesting features: the values of the correlation energy are comparable with that of the free helium atom and increase for all cases as ω increases. The percentage of the correlation energy of quantum dots is, in all cases, much larger than that for the free helium atom of approximately 1% for weak confinement. This confirms the importance of electron correlation in the singlet states of quantum dots as already observed in previous studies [29, 38, 39]. Its percentage decreases in all cases with increasing ω, and consequently electron correlation becomes less important for strong confinement [29, 38]. This is consistent with the observation made above that configuration mixing is stronger for $\omega = 0.1$ than for $\omega = 0.5$.

The percentage of correlation energy of the spherical quantum dot is considerably smaller than that of the prolate and the oblate quantum dots. This observation may be rationalized by the effect of dimensionality [39]. As demonstrated previously for the rectangular box model [38] and for the two-dimensional and three-dimensional harmonic oscillator quantum dots [39], electron correlation plays a much larger role in the low-dimensional systems than in the corresponding three-dimensional systems. In the limit the prolate and the oblate harmonic oscillator quantum dots discussed above become one-dimensional and two-dimensional quantum systems, respectively. Therefore, these systems have larger electron correlation than the corresponding spherical quantum dot.

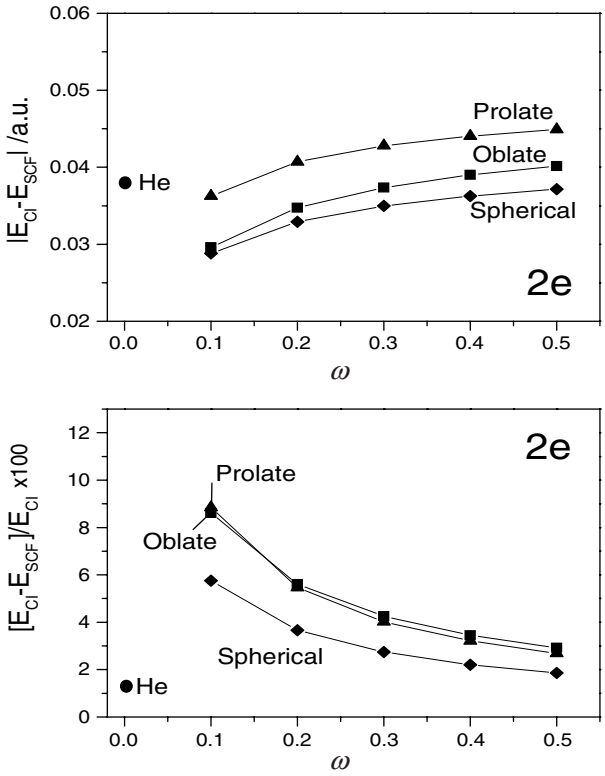

Figure 16. Correlation energy of a spherical, a prolate and an oblate quantum dot as a function of ω.

4. Summary

The spectrum, electron-density distribution and ground-state correlation energy of two electrons confined by a spherical, a prolate and an oblate harmonic oscillator potential with different values of ω have been studied by using the quantum-chemical CI method employing a Cartesian *anisotropic* Gaussian basis set and a full CI wavefunction. The most important results of this study are summarized as follows: a Cartesian *anisotropic* Gaussian basis set is required to correctly approximate the electronic wavefunction of quantum systems confined in an *anisotropic* harmonic oscillator potential. The total energy and spacing between energy levels increases in all cases with increasing confinement strength ω. The energy level structure cannot be matched by scaling with respect to ω. For spherical quantum dots the sequence of states is the same within the range of ω studied. For prolate and oblate quantum dots the sequence of states may vary for different values of ω. The electron-density distribution becomes more and more compressed for increasing confinement strength. The correlation energy of the ground state is comparable in magnitude to that of the helium atom. It increases for increasing ω. The percentage of the correlation energy with respect to the total energy of the ground state is considerably larger than that of the helium atom. For the spherical quantum dot it is considerably smaller than for the other cases. The correlation energy for the prolate and oblate quantum dots differs considerably while its percentage is nearly identical.

Acknowledgment

One of the authors (TS) thanks the Alexander von Humboldt Foundation for a Research Fellowship.

References

[1] Ashoori R C 1996 *Nature* **379** 413–19
[2] Johnson N F 1995 *J. Phys.: Condens. Matter* **7** 965–89
[3] Tarucha S, Austing D G, Honda T, van der Hage R T and Kouwenhoven L P 1996 *Phys. Rev. Lett.* **77** 3613–16
[4] Tang Z K, Nozue Y and Goto T 1992 *J. Phys. Soc. Japan* **61** 2943–50
[5] Cioslowski J and Fleischmann E D 1991 *J. Chem. Phys.* **94** 3730–4
[6] Baltenkov A S 1999 *J. Phys. B: At. Mol. Opt. Phys.* **32** 2745–51
[7] Takami M 1996 *Comment. At. Mol. Phys.* **32** 219–31
[8] Fock V 1928 *Z. Phys.* **47** 446–8
[9] Darwin C G 1930 *Proc. Camb. Phil. Soc.* **27** 86–90
[10] Taut M 1993 *Phys. Rev.* A **48** 3561–6
[11] Ghosh S K and Samanta A 1991 *J. Chem. Phys.* **94** 517–22
[12] Merkt U, Huser J and Wagner M 1991 *Phys. Rev.* B **43** 7320–3
[13] Jaskólski W 1996 *Phys. Rep.* **271** 1–66
[14] Connerade J P, Dolmatov V K and Lakshmi P A 2000 *J. Phys. B: At. Mol. Opt. Phys.* **33** 251–64
[15] Zicovich-Wilson C, Planelles J H and Jaskólski W 1994 *Int. J. Quantum Chem.* **50** 429–44
[16] Friedrich H and Wintgen D 1989 *Phys. Rep.* **183** 37–79
[17] Krähmer D S, Schleich W P and Yakovlev V P 1998 *J. Phys. A: Math. Gen.* **31** 4493–520
[18] Changa M E, Scherbinin A V and Pupyshev V I 2000 *J. Phys. B: At. Mol. Opt. Phys.* **33** 421–32
[19] Dutt R, Mukherjee A and Varshni Y P 2001 *Phys. Lett.* A **280** 318–24
[20] Patil S H 2001 *J. Phys. B: At. Mol. Opt. Phys.* **34** 1049–58
[21] Mateos-Cotès S, Ley-Koo E and Cruz S A 2002 *Int. J. Quantum Chem.* **86** 376–89
[22] Banerjee A, Sen K D, Garza J and Vargas R 2002 *J. Chem. Phys.* **116** 4054–7
[23] Bednarek S, Szafran B and Adamovski J 1999 *Phys. Rev.* B **59** 13036–42
[24] Ezaki T, Mori N and Hamaguchi C 1997 *Phys. Rev.* B **56** 6428–31
[25] Koskinen M, Manninen M and Reimann S M 1997 *Phys. Rev. Lett.* **79** 1389–92
[26] Lee I, Rao V, Martin R M and Leburton J 1998 *Phys. Rev.* B **57** 9035–42
[27] Henderson T M, Runge K and Bartlett R J 2001 *Chem. Phys. Lett.* **337** 138–42
[28] Peeters F M 1990 *Phys. Rev.* B **42** 1486–7
[29] Pfannkuche D, Gudmundsson V and Maksym P 1993 *Phys. Rev.* B **47** 2244–50
[30] Fujito M, Natori A and Yasunaga H 1996 *Phys. Rev.* B **53** 9952–8
[31] Müller H M and Koonin S E 1996 *Phys. Rev.* B **54** 14532–9
[32] Harju A, Sverdlob V A and Nieminen R M 1999 *Phys. Rev.* B **59** 5622–6
[33] Yannouleas C and Landman U 1999 *Phys. Rev. Lett.* **82** 5325–8
[34] Adamowski J, Sobkowicz M, Szafran B and Bednarek S 2000 *Phys. Rev.* B **62** 4234–7
[35] Cioslowski J and Pernal K 2000 *J. Chem. Phys.* **113** 8434–43
[36] Yannouleas C and Landman U 2000 *Phys. Rev.* B **61** 15895–904
[37] McCarthy S A, Wang J B and Abbott P C 2001 *Comput. Phys. Commun.* **141** 175–204
[38] Bryant G W 1987 *Phys. Rev. Lett.* **59** 1140–3
[39] Rontani M, Rossi F, Manghi F and Molinari E 1999 *Phys. Rev.* B **59** 10165–75
[40] Connerade J P and Dolmatov V K 1998 *J. Phys. B: At. Mol. Opt. Phys.* **31** 3557–64
[41] Cruz S A and Soullard J 2001 *Int. J. Quantum Chem.* **83** 271–8
[42] Rivelino R and Vianna J D M 2001 *J. Phys. B: At. Mol. Opt. Phys.* **34** L645–50
[43] Szafran B, Adamoeski J and Stébé B 1998 *J. Phys.: Condens. Matter* **10** 7575–86
[44] Szafran B, Adamowski J and Bednarek B 1999 *Physica* E **4** 1–10
[45] Szafran B, Adamowski J and Bednarek B 2000 *Physica* E **5** 185–95
[46] Bielińska-Wąż D, Karwowski J and Diercksen G H F 2001 *J. Phys. B: At. Mol. Opt. Phys.* **34** 1987–2000
[47] Bielińska-Wąż D, Diercksen G H F and Klobukowski M 2001 *Chem. Phys. Lett.* **349** 215–19
[48] Sako T and Diercksen G H F 2003 *J. Phys.: Condens. Matter* to be submitted
[49] Fluegge S 1971 *Practical Quantum Mechanics* (Berlin: Springer)
[50] Diercksen G H F and Hall G 1994 *Comput. Phys.* **8** 215
[51] Sako T and Diercksen G H F 2003 *J. Phys. B: At. Mol. Opt. Phys.* **36** 1433–57
[52] Sako T and Diercksen G H F 2003 *J. Phys. B: At. Mol. Opt. Phys.* **36** 1681–702
[53] Wilson S 1984 *Electron Correlation in Molecules* (Oxford: Clarendon)